observed in the experimental system when oscillation frequency was equal or lower than 0.167 Hz. In such a case attempts to achieve a complete consumption of the limiting reactant (complete decolouration of phenolphthalein) in a reasonable time (4÷5 hours) failed.
For higher oscillation frequencies, when inert forces become comparable with viscous forces, one should observe gradually increasing differences in the shape of the base zone after a few oscillation cycles; as it took place in the experimental system when oscillation frequency was equal to 0.333 Hz. Introduction of any obstacles in the flow domain may considerably amplify the action of the inert forces and accelerate convective mixing. This thesis was fully confirmed by the experimental results; compare 42% selectivity obtained when no baffle was mounted in the reactor with 36.4% and 29.0% selectivity achieved when respectively 5.5 mm and 18 mm baffle was inserted in the gap. Analysis of figure 8.11 shows additionally, that decreasing of the oscillation frequency not only elevates the final selectivites but also decreases differences between the selectivities obtained for two different baffle widths.

8.3. Modelling of Micromixing in the Batch Reactor.

The differential material balances of the substrates of competitive-parallel reactions:

$$A + B \overset{k_1}{\rightarrow} P \qquad \text{with} \quad k_1 \rightarrow \infty \,, \tag{5.34a}$$

$$A + C \overset{k_2}{\rightarrow} Q \qquad \text{and} \quad R_i = -k_2 \cdot c_A \cdot c_C \tag{5.34b}$$

in a local coordinate system, attached to the symmetry plane of a layer containing reactant **A**, with the boundary and initial conditions have the following form:

$$\frac{\partial c_i}{\partial t} + \frac{x}{s} \cdot \frac{ds}{dt} \cdot \frac{\partial c_i}{\partial x} = D_i \cdot \frac{\partial^2 c_i}{\partial x^2} - k_2 \cdot c_A \cdot c_C \,, \qquad \text{where} \quad i = A, C \,, \tag{8.20a}$$

$$\frac{\partial c_B}{\partial t} + \frac{x}{s} \cdot \frac{ds}{dt} \cdot \frac{\partial c_B}{\partial x} = D_B \cdot \frac{\partial^2 c_B}{\partial x^2} \,, \tag{8.20b}$$

- at plane $x = 0$ $\qquad \dfrac{\partial c_A}{\partial x} = \dfrac{\partial c_C}{\partial x} = 0 \,,$ **(8.20c)**

- at plane $x = s$ $\qquad \dfrac{\partial c_B}{\partial x} = \dfrac{\partial c_C}{\partial x} = 0 \,,$ **(8.20d)**

- at instantaneous reaction plane $x = x_R$

$$c_A = c_B = 0 \,, \qquad D_A \cdot \frac{\partial c_A}{\partial x} + D_B \cdot \frac{\partial c_B}{\partial x} = 0 \,, \tag{8.20e}$$

$$c_A(x,0) = \begin{cases} c_{A0} & 0 \le x < \delta_0/2 \\ 0 & \delta_0/2 \le x \le s_0 \end{cases} , \tag{8.20f}$$

$$c_i(x,0) = \begin{cases} 0 & 0 \le x \le \delta_0/2 \\ c_{i0} & \delta_0/2 \le x \le s_0 \end{cases} , \qquad \text{where} \quad i = B,C . \tag{8.20g}$$

For the case of test reactions (6.1), symbols **A**, **B** and **C** represent NaOH, HCl and $CH_2ClOOC_2H_5$, respectively. Using dimensionless variables (5.101) one can get rid of convective terms in equations (8.20ab). Eventually, one receives:

$$\frac{\partial C_i}{\partial \tau} = \frac{D_i}{D_A} \cdot \frac{\partial^2 C_i}{\partial \xi^2} - Da \cdot \left(\frac{s}{s_0}\right)^2 \cdot C_A \cdot C_C , \qquad \text{where} \quad i = A,C , \tag{8.21a}$$

$$\frac{\partial C_B}{\partial \tau} = \frac{D_B}{D_A} \cdot \frac{\partial^2 C_B}{\partial \xi^2} , \tag{8.21b}$$

- at plane $\xi = 0$ $$\frac{\partial C_A}{\partial \xi} = \frac{\partial C_C}{\partial \xi} = 0 , \tag{8.21c}$$

- at plane $\xi = 1$ $$\frac{\partial C_B}{\partial \xi} = \frac{\partial C_C}{\partial \xi} = 0 , \tag{8.21d}$$

- at instantaneous reaction plane $\xi = \xi_R$

$$C_A = C_B = 0 , \qquad \frac{\partial C_A}{\partial \xi} + \frac{D_B}{D_A} \cdot \frac{\partial C_B}{\partial \xi} = 0 , \tag{8.21e}$$

$$C_A(\xi,0) = \begin{cases} 1 & 0 \le \xi < \dfrac{\delta_0}{2s_0} \\ 0 & \dfrac{\delta_0}{2s_0} \le \xi \le 1 \end{cases} , \tag{8.21f}$$

$$C_i(\xi,0) = \begin{cases} 0 & 0 \le \xi \le \dfrac{\delta_0}{2s_0} \\ \dfrac{c_{i0}}{c_{A0}} & \dfrac{\delta_0}{2s_0} \le \xi \le 1 \end{cases} , \qquad \text{where} \quad i = B,C . \tag{8.21g}$$

In equations (8.21) symbol **Da** stands for Damköhler number:

$$Da = k_2 \cdot s_0^{\,2} \cdot c_{A0} / D_A , \tag{8.22}$$

A method of gradient concentration moments described in chapter 5.2 was applied to transform equations (8.21). Integral moments defined as follows:

$$M_j^{\,i} = \int_{a_i(\tau)}^{b_i(\tau)} \xi^j \cdot \frac{\partial C_i}{\partial \xi} d\xi \ , \qquad i = A, B, C \ , \tag{8.23}$$

where the integration limits are:

- for reactant A $\quad a_A = 0 \ , \quad b_A = \xi_R \ ,$ **(8.24a)**

- for reactant B $\quad a_B = \xi_R \ , \quad b_B = 1 \ ,$ **(8.24b)**

- for reactant C $\quad a_C = 0 \ , \quad b_C = 1 \ ,$ **(8.24c)**

were substituted into equations (8.21ab), integrated in the interval $0 \le \xi \le 1$ with weight functions ξ^j. Using this procedure a system of four equations was obtained:

$$\frac{dM_A^{\,1}}{d\tau} = -\left.\frac{\partial C_A}{\partial \xi}\right|_{\xi_R} + Da \cdot \left(\frac{s}{s_0}\right)^2 \cdot \int_0^{\xi_R} C_A \cdot C_C d\xi \ , \tag{8.25a}$$

$$\frac{dM_B^{\,1}}{d\tau} = \left.\frac{dC_B}{d\tau}\right|_{\xi=1} + \frac{D_B}{D_A} \cdot \left.\frac{\partial C_B}{\partial \xi}\right|_{\xi_R} \ , \tag{8.25b}$$

$$\frac{dM_C^{\,1}}{d\tau} = \left.\frac{dC_C}{d\tau}\right|_{\xi=1} + Da \cdot \left(\frac{s}{s_0}\right)^2 \cdot \int_0^{\xi_R} C_A \cdot C_C d\xi \ , \tag{8.25c}$$

$$\frac{dM_C^{\,2}}{d\tau} = \left.\frac{dC_C}{d\tau}\right|_{\xi=1} + 2 \cdot \frac{D_C}{D_A} \cdot \left(C_C|_{\xi=1} - C_C|_{\xi=0}\right) + 2 \cdot Da \cdot \left(\frac{s}{s_0}\right)^2 \cdot \int_0^{\xi_R} \xi \cdot C_A \cdot C_C d\xi \ . \tag{8.25d}$$

To close the system of equations (8.25) one can approximate the reactant profiles with two parameter "linear" functions [74]. As a result, one obtains the system of four ordinary differential equations (transformed equations (8.25)) and the boundary condition at the reaction plane (transformed equations (8.21e)), which can be solved by means of the backward Euler scheme - for detailed description see appendix E.

As it was shown earlier, the distance between the symmetry planes of the neighbouring reactant layers, **s**, depends on the radial position in the annular gap. Thus in computations, **s** was replaced with $\bar{s}$ - expression (8.16), s_0 was replaced by $\bar{s}_0$ - expression (8.18) and the "warped time" was related to the real time by expression (8.17).

A comparison of model and experimental results was conducted for the first and second series of tests. Diffusivity coefficients necessary for computations were obtained from experimental correlations (6.13)÷(6.15). As a result, it was obtained $D_A = 4.51 \cdot 10^{-10}$ m^2/s (NaOH), $D_B = 9.95 \cdot 10^{-10}$ m^2/s (HCl) and $D_C = 0.0943 \cdot 10^{-10}$ m^2/s ($CH_2ClCOOC_2H_5$). The rate constant of

ester hydrolysis at 18°C equals 23.7 $dm^3/(mol \cdot s)$.

Figure 8.12 presents the comparison of the final selectivities, measured and calculated for different shear rates in the annular gap. The computed selectivities are slightly higher than the measured ones, except one point obtained for the lowest shear rate; the model predicts a weaker influence of the shear rate on the product distribution.

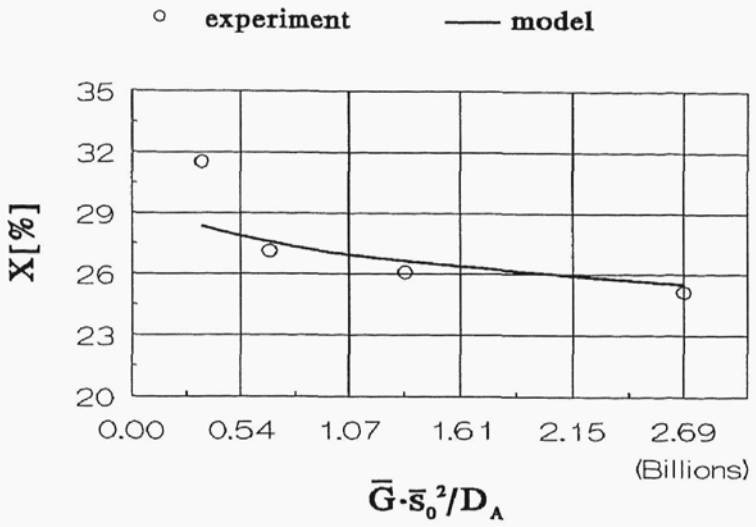

Figure 8.12. Effect of the shear rate on the final selectivity in the batch reactor; $Da/(1+a)=4.787 \cdot 10^7$, $a=7$.

It was determined experimentally that the value of initial volume ratio can strongly influence the product distribution. A comparison of experimental and theoretical results, presented in figure 8.13, proves that the model also predicts this effect. It can be noticed, however, that the model predicts stronger effect of the initial volume ratio on the final selectivity than it was determined experimentally.

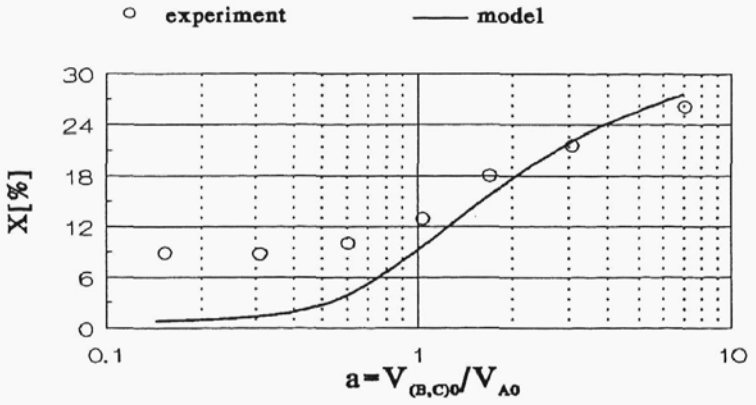

Figure 8.13. Effect of the volume ratio on the final selectivity in the batch reactor; $Da/(1+a)=4.787 \cdot 10^7$, $\bar{G} \cdot \bar{s}_0^2/D_A=6.717 \cdot 10^8$.

To explain discrepancies between the computed and measured selectivities one should take into account that the model uses very simple, two parameter functions for approximation of the reactant concentration profiles. Besides, the Couette flow created in the experimental system, tends to orient contact surfaces between the mixed liquids along the direction of shear. When this happens, usually after a few revolutions of the inner cylinder, molecular diffusion becomes less and less enhanced by the deformation of the reactant layers - the rate of mass transfer is then directly proportional to the reactants diffusivity. Thus, even a few percent error committed during the determination of a coefficient of molecular diffusivity of any reactant may strongly affect the computed product distribution. Finally, it should be pointed out that

such model parameters as $\bar{G}$, $\bar{s}$ and $\bar{s}_0$ were determined from theoretical expressions (8.15), (8.16) and (8.18); there was no fitting of the model parameters to experimental data.

Except the final selectivity, the model of the gradient concentration moments allows to determine the time required to complete test reactions (6.1) in the batch mixer from equations (8.16) and (8.17). This time can be used to compute energetic efficiency of mixing in the experimental system. The local efficiency of mixing in shear flow can be determined directly from definition (2.67) - [47]:

$$eff(t) = \sqrt{2} \cdot G \cdot t / \left(1 + G^2 \cdot t^2\right) . \tag{8.26}$$

At the beginning of the process, when the intermaterial surface is perpendicular to direction of shear, efficiency equals zero. Later, when the intermaterial surface becomes oriented along direction of the fastest stretch in the shear flow (**t=1/G**), efficiency reaches its maximum equal to 0.707. For time longer than **t=1/G** the value of efficiency becomes inversely proportional to time. The average value of **eff(t)** in time $\mathbf{t_f}$ equals:

$$\overline{eff(t_f)} = \frac{1}{t_f} \cdot \int_0^{t_f} eff(t')\,dt' = \ln\left(1 + G^2 \cdot t_f^2\right) \Big/ \left(\sqrt{2} \cdot G \cdot t_f\right) . \tag{8.27}$$

In the experimental system the shear rate depends on the radial position - equation (8.4). In order to compute the average efficiency in the entire liquid volume, one should replace, in equation (8.27) the local value of **G** with its average $\bar{G}$ given by expression (8.15):

$$\left\langle eff(t_f) \right\rangle_V = \ln\left(1 + \bar{G}^2 \cdot t_f^2\right) \Big/ \left(\sqrt{2} \cdot \bar{G} \cdot t_f\right) . \tag{8.28}$$

Tables 8.VII and 8.VIII report the reaction times and the mean efficiency values calculated for the first and the second series of tests.

Table 8.VII. Effect of the rotational speed on the energetic efficiency of mixing.

n [rev/min]	5	10	20	40
t_f [s]	232.5	147.6	93.8	59.8
$\langle eff(t_f) \rangle_V$	0.0181	0.0148	0.0121	0.0098

Table 8.VIII. Effect of the initial volume ratio on the energetic efficiency of mixing.

a	1/7	1/3	3/5	1	5/3	3	7
t_f [s]	217.9	210.6	198.1	182.8	170.4	158.9	147.6
$\langle eff(t_f) \rangle_V$	0.0106	0.0109	0.0115	0.0123	0.0131	0.0139	0.0148

Analysis of these tables shows that decreasing the mixing time, t_f, raises the energetic efficiency of mixing in the reactor. On the other hand, a comparison of mixing efficiencies with the final selectivities indicates that the most effective use of mechanical energy may not result in better mixing. To sum it up, one should rather minimize the total energy input required to obtain a desired result than maximize the energetic efficiency of mixing, in order to find the optimal processing conditions.